Nanoscale

Accepted Manuscript

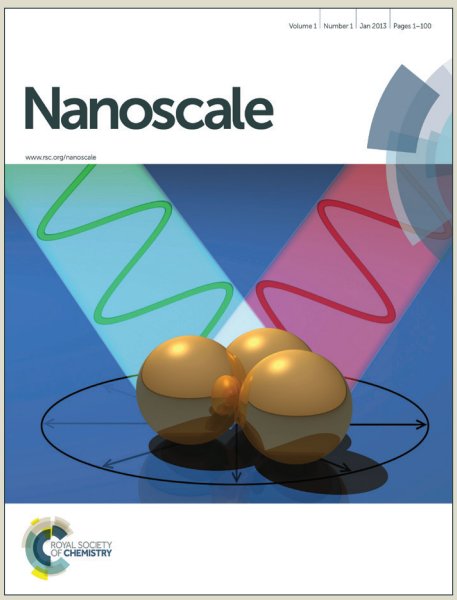

ROYAL SOCIETY OF CHEMISTRY

www.rsc.org/nanoscale

Mesoporous Persistent Nanophosphors for In vivo Optical Bioimaging and Drug-delivery

Thomas Maldiney,[a] *Benoit Ballet,*[a] *Michel Bessodes,*[a] *Daniel Scherman,*[a] *Cyrille Richard,*[a,]*

[a] Unité de Technologies Chimiques et Biologiques pour la Santé (UTCBS), CNRS UMR 8258, INSERM U 1022, Paris, F-75270 cedex France; Université Paris Descartes, Sorbonne Paris Cité, Faculté des Sciences Pharmaceutiques et Biologiques, Paris, F-75270 cedex France; ENSCP, Paris, F-75231 cedex France.

cyrille.richard@parisdescartes.fr

ABSTRACT. Based upon the ambitious idea that one single particle could serve multiple purposes at the same time, the combination and simultaneous use of both imaging and therapeutic lately arouse as one of the most promising perspective among nanotechnologies directed toward biomedical applications. Intended for both therapeutics and diagnostics *in vivo*, highly complex nanostructures were specifically designed to simutaneously act as optical imaging probe and delivery vehicle. Yet, such multifunctional photonic nanoplatforms usually exploit fluorescence phenomena which require constant excitation light through biological tissues and thus significantly reduce detection sensitivity due to the autofluorescence from living animals. In order to overcome this critical issue, the present article introduces a novel multifunctional agent based on persistent luminescence mesoporous nanoparticles. Composed of a hybrid chromium-doped zinc gallate core/mesoporous silica shell architecture, we show that this nanotechnology can be used as efficient doxorubicin-delivery vehicle presenting higher cytotoxicity toward U87MG cells than its unloaded counterpart *in vitro*. In addition, we demonstrate that persistent luminescence signal from these doxorubicin-loaded mesoporous persistent nanophosphors

opens alternative to highly sensitive detection *in vivo*, giving access to the real-time biodistribution of the carrier without any autofluorescence from the animal tissues. This new persistent luminescence-based hybrid nanotechnology should easily be transposed to the delivery of any therapeutic agent, thus constituting a versatile and sensitive optical nanotool dedicated to both therapeutic and diagnosis applications *in vivo*.

KEYWORDS. Persistent luminescence, Nanoparticle, Mesoporous, Silica, Optical Imaging, In vivo, Doxorubicin, Drug delivery.

MANUSCRIPT TEXT.

Introduction. Along with the development of highly sophisticated and rationally designed nanocarriers[1,2], the idea of theranostic has recently emerged as an efficient way to combine diagnostics-therapeutics purposes into one single multifunctional nanoplatform[3,4]. One of the main advantages usually claimed about cargo systems in the nanometer scale relies in their ability to avoid renal filtration[5], successfully circulate in the blood for several hours[6], and significantly improve efficient targeting to the tissues of interest[7]. Based on its relative low cytotoxicity and excellent chemical stability, mesoporous silica is very certainly one of the most referred inorganic hosts for the design of hybrid nanostructures intended for biomedical applications[8,9,10]. Indeed, due to poor porosity parameters and low specific surface areas associated with their synthesis, common inorganic/imaging nanoprobes-based theranostic agents generally exploit the translational properties of silica for the synthesis of a single mesoporous core-shell architecture[11,12]. Such approach has already been envisioned with various imaging modalities, from magnetic resonance imaging[13,14] (MRI) to optical imaging[15,16]. In the latter case, the use of classical fluorescence-based techniques, which require constant illumination of the emitting centers, most often preclude sensitive detection of the hybrid constructions *in vivo* due to the undesirable autofluorescence from living tissues[17]. Upconversion nanoparticles encapsulated in mesoporous silica are currently being envisioned as optical alternative to common photonic theranostic

agents[18]. Unfortunately, there is still to our knowledge no report of this technology for *in vivo* observations in small animals.

Our group lately introduced the use of persistent luminescence nanoparticles *in vivo*, for the optical imaging of vascularization in living mice[19,20]. Designed to circumvent the autofluorescence from living tissues and enable highly sensitive detection, this nanotechnology has already demonstrated its versatility for various applications *in vivo*[21,22] and positive results for the specific targeting of several cancer cells *in vitro*[23,24] or *in vitro* inhibition assay[25]. However, despite successful optimization of the initial composition[26], persistent luminescence could not be activated *in situ*, preventing long-term observations in living animals. This critical limitation was recently overcome by the discovery of a series of novel nanophosphors[27,28] among which $ZnGa_{1.995}Cr_{0.005}O_4$, referred to as ZGO, whose persistent luminescence can be activated *in vivo*, under a simple orange-red LEDs source, through living tissues. In additions, this last generation of persistent luminescence nanoparticles demonstrated neither acute nor long-term *in vivo* toxicity following biomarkers dosage from liver as well as histopathological tissue analysis of the main RES organs.[29]

The present article introduces a multifunctional nanoplatform based on persistent luminescence nanoparticles for both *in vivo* optical imaging and drug delivery. Taking advantage of the well-known biocompatibility of mesoporous silica[30] and non-toxic ZGO,[29] we modeled a novel core-shell structure on the basis of hybrid chromium-doped zinc gallate/mesoporous silica architecture specifically designed to allow both highly sensitive optical detection through living tissues and concomitant drug delivery. Employing doxorubicin as a drug model for the purpose of this study, we demonstrate that these mesoporous persistent nanophosphors can be successfully loaded with an anticancer agent, and subsequently initiate its progressive release in a pH-sensitive manner. The use of such doxorubicin-loaded theranostic agent is finally shown to induce acute cytotoxicity toward U87MG cells *in vitro*, preserve persistent luminescence properties, and allow both sensitive and non invasive localization of the carrier *in vivo*.

Results and discussion. Monodisperse crude ZGO nanoparticles were extracted from a polydisperse powder synthesized by a two-step method combining a hydrothermal treatment followed by a low-temperature sintering in air at 750°C for 5 hours. These nanophosphors, already described in a previous work[29,22], displayed bright near-infrared persistent luminescence centered on 700 nm (data not shown), low porosity (Table 1) and an average hydrodynamic diameter of 85 mn (Table 2). The condensation of tetraethylortosilicate (TEOS), in the presence of cetyltrimethylammonium bromide (CTAB), on the surface of ZGO nanoparticles allowed the formation of ZGO@SiO_2 nanoparticles according to Scheme 1. Due to a relative sensitivity of ZGO nanoparticles to acidic solutions, the extraction of CTAB was performed in a 1% solution of NaCl in methanol. We notice from Table 1 that the number of extraction steps has a critical influence on the final specific surface area of the compound. After a proper extraction of the structure directing agent, the ZGO@SiO_2 nanocomposite was characterized by a large specific surface area of more than 400 m^2/g (Table 1), calculated from the N_2 adsorption/desorption isotherms (Fig. 1.a) and the BET plot curve (Supplementary Fig. S1), as well as an average pore size approaching 2 nm (Fig 1.b). Noteworthy, increasing the number of extraction steps was not responsible for any increase of the specific surface area (data not shown) which demonstrates the complete extraction of CTAB. These results, in the same order of magnitude as other hybrid nanocarriers based on mesoporous silica[31], confirm the formation of a mesoporous architecture with relative high specific surface area. The core-shell structure, was assessed by transmission electron microscopy (TEM) before (Fig. 2.a) and after the formation of the mesoporous silica shell (Fig. 2.b and c). The photomicrographs allow to clearly distinguish the zinc gallate core, that appears as a dark spot on the cliché, embedded in a mesoporous silica shell, discovering a lighter thickness around the core. Besides, we notice that most of the silica shells are filled with one ZGO core, which is the result of a precise control of TEOS concentration[32]. To this end, the synthesis was adapted according to the protocol described by Joo et al. for the synthesis of magnetic mesoporous nanoparticle nanoparticles.

Physico-chemical characterization of ZGO@SiO_2 nanoparticles are displayed in Table 2 and indicate a significant evolution of the hydrodynamic diameter after encapsulation of the ZGO core into the silica

shell. Nanoparticles core diameter increases from 84 nm, for the ZGO core, to 163 nm for the final ZGO@SiO_2 nanoparticles. Along with an important evolution of the nanoparticle size, the encapsulation of ZGO crystals in mesoporous silica goes with a substantial change in surface properties. Indeed, Ga-OH functional groups, on the surface of the initial ZGO nanoparticles, were responsible for a slightly positive charge at neutral pH (Table 2). The condensation of TEOS on the surface of ZGO nanoparticles not only masked these Ga-OH groups, but also created a preeminant silanol-based structure, decorated by Si-OH groups, accountable for the final negative charge of ZGO@SiO_2 nanoparticles. To further characterize these surface properties of the silica shell, in comparison to the zinc gallate core, we studied the evolution of the surface charge as a function of pH. The resuting curves, displayed in Supplementary Fig. S2, allow to evaluate the point of zero charge (PZC) associated with each structure. As expected from the first measurements of zeta potential in 20 mM NaCl solution, the PZC of ZGO nanoparticles is much higher (~7.5) than that of ZGO@SiO_2 nanocomposites (<1), which is in total agreement with the reported values for gallium oxide[33] and silica[34]. Noteworthy regarding the putative application of such mesoporous structure for diagnostics in living animals, the formation of such silica mesoporous shell around ZGO nanoparticles had only poor influence on the persistent luminescence properties of the chromium-doped zinc gallate crystals (data not shown).

In order to demonstrate the potential interest of ZGO@SiO_2 as efficient nanocarrier, we have chosen doxorubicin as a model drug, evaluated the entrapment efficiency of our system, and measured its ability to release the drug from the mesoporous structure, depending on the pH conditions. The pKa of doxorubicin being 8.6, the entrapment could be envisioned in PBS (pH = 7.4). The strong negative charge from silanol groups at that pH make them very likely to interact with positively charged doxorubicin, via classical electrostatic interactions. The loading content, defined as the weight of doxorubicin in ZGO@SiO_2 in relation to the weight of doxorubicin-loaded ZGO@SiO_2, was determined to be of 49 %. This value, which was found to be almost identical to the highest loading content obtained by Yuan et al. for the adsorption of doxorubicin in mesoporous silica nanoparticles[35] (MSNs), confirmed the high loading capacity of our hybrid ZGO@SiO_2 system. Practically, the entrapment of

doxorubicin was assessed by exploiting the strong absorption of doxorubicin at 480 nm (Supplementary Fig. S3). The respective absorptions of ZGO@SiO_2 and ZGO@SiO_2-Dox suspended in PBS were compared with a UV-visible spectrophotometer. Results from Fig. 3.a indicate a strong absorption of the loaded nanocarriers ZGO@SiO_2-Dox at 480 nm, in comparison to the empty ZGO@SiO_2 nanoparticles, which attested to the presence of doxorubicin. The comparison of physico-chemical parameters of the nanocarrier before and after doxorubicin loading revealed a significant increase of the hydrodynamic diameter, evolving from 163 nm for ZGO@SiO_2 nanoparticles to 185 nm for ZGO@SiO_2-Dox nanoparticles (Table 2). Such slight increase of the hydrodynamic diameter after doxorubicin-loading is very certainly the result of a change in the solvatation sphere due to the presence of doxorubicin on the surface of the nanoparticles, and the concomitant adaptation of the system colloidal stability. This little evolution of the colloidal geometry also comes with a radical shift of the zeta potential value, increasing from -27 mV to 13 mV. Upon the addition of doxorubicin in PBS, the negative silanol groups of the mesoporous silica host progressively cover with the positive charges of the encapsulated drug. In the end, the surface of ZGO@SiO_2-Dox nanoparticles is completely decorated with doxorubicin, responsible for the global positive charge of the drug-containing carrier. Given the significant visible absorption from the loaded doxorubicin, we also studied the influence of doxorubicin-loading on both UV and orange-red excitability of the persistent luminescence signal from ZGO@SiO_2 nanoparticles. The persistent luminescence decay curves in Fig. 3.b first indicate that the doxorubicin is not responsible for any total quenching of persistent luminescence signal. Yet, ZGO@SiO_2-Dox nanoparticles displayed a persistent luminescence signal rather diminished compared to their empty counterpart. The signal loss between ZGO@SiO_2 and ZGO@SiO_2-Dox is dependent on the excitation energy, leading to a four times decrease after UV excitation and half this factor following LEDs activation. This wavelength-dependent signal loss can be explained by the optical properties of doxorubicin and more precisely its preferential UV absorption compared to red light, attested by the UV-Vis absorption spectrum from Supplementary Fig. S3.

Prior to comparing the cytotoxicity of ZGO@SiO_2 and ZGO@SiO_2-Dox, we determined the doxorubicin release behavior associated with our mesoporous persistent nanophosphors as a function of pH. The releasing profiles, shown in Supplementary Fig. S4, confirm a clear pH-dependency of the drug release rate, with an increased release for the lowest pH. The cumulative release of doxorubicin at pH 5 reached a little more than 25 % of the initial doxorubicin content after a 30 hours period. In PBS, the release only increased up to half this value after the same period of time. Such profiles reflect the electrostatic interaction between doxorubicin and mesoporous silica and are very similar to those reported by Yuan et al. in their study about MSNs[35].

These drug release properties of ZGO@SiO_2-Dox were then exploited for *in vitro* cell assay on U87MG and comparison of the cytotoxicity induced by doxorubicin alone, ZGO@SiO_2 nanoparticles and their loaded counterpart ZGO@SiO_2-Dox. Relative U87MG cell viability assay from Fig. 4.a indicate an IC50 value (the concentration of drugs required to reduce cell growth by 50 %) of free DOX equal to approximately 12.5 µg/mL, which corresponds to a doxorubicin concentration of 23 µM, in the same order of magnitude as the one reported by Kumar et al. on the same cell line[36]. Interestingly, the assay with ZGO@SiO_2 revealed no acute cytotoxicity of the nanoparticles up to 250 µg/mL, which approximately corresponds to the value of the IC50 (Fig. 4.b). The same assay with ZGO@SiO_2-Dox nanoparticles confirms the cytotoxic effect of the entrapped drug. Indeed, the introduction of doxorubicin into the silica shell of ZGO@SiO_2 nanoparticles causes the IC50 to drastically decrease from 250 µg/mL to approximately 5 µg/mL, which represents a doxorubicin concentration of 9 µM. When comparing this last value to the one obtained with the free drug, we notice that the IC50 of ZGO@SiO_2-Dox nanoparticles represents less than half the IC50 of free doxorubicin. This result not only demonstrates the ability to use this hybrid zinc gallate/mesoporous silica platform as efficient nanocarrier for the vectorization of anticancer drugs and treatment *in vitro*, but also confirms the relative benefit of encapsulating doxorubicin within ZGO@SiO_2 nanoparticles, responsible for a significant decrease of the IC50 value in comparison to free doxorubicin. Despite such promising results *in vitro*, one of the most demanding challenge regarding multifunctional platforms still relies in the ability to

properly detect these theranostic agents *in vivo*, i.e. with good sensitivity, but also successfully monitor their biodistribution and accumulation sites through living tissues.

For this reason, we finally studied as a proof of concept the ability to use the persistent luminescence signal from zinc gallate-cores to follow the real-time biodistribution of the drug-loaded ZGO@SiO_2-Dox nanoparticles *in vivo*. The persistent luminescence images, acquired after the systemic administration of 2 mg of doxorubicin-loaded mesoporous persistent nanophosphors, clearly demonstrate the optical potential of such technology in living animals (Fig. 5.a). Interestingly, the recourse to persistent luminescence allows complete avoidance of the autofluorescence from biological tissues and highly sensitive detection through living tissues. From the chronological observation of the images in Fig. 5.a, we notice the appearance of a rapid tropism associated with the biodistribution of ZGO@SiO_2-Dox nanoparticles. A few seconds after the injection, most of the signal is located in the lungs, which corresponds to first vascularized organs following a tail vein injection. Within a few minutes only, the biodistribution profile quickly evolves from the lungs to the liver. After 15 minutes, almost all the signal from ZGO@SiO_2-Dox nanoparticles is located in the liver area. Such accumulation pattern is highly representative of charged nanoparticles, widely known to undergo a rapid sequestration within major organs of the reticulo-endothial system, mainly liver and spleen[19,20]. Image-based semi-quantitative biodistribution within liver and lungs brings additional information concerning the recognition/uptake kinetics of ZGO@SiO_2-Dox nanoparticles by Kupffer cells from the liver (Fig. 5.b). It also shows that the biodistribution freezes 20 minutes after the injection, leaving up to 80 % of the signal from the whole mouse retained in the liver. This accumulation profile was confirmed 24 hours post-injection by the whole-mouse *in vivo* biodistribution (Supplementary Fig. S5.a), obtained after *in situ* activation of persistent luminescence signal from ZGO@SiO_2-Dox nanoparticles with the LEDs system, and by the *ex vivo* biodistribution established from the harvested organs (Supplementary Fig. S5.b and c). Although these first results *in vivo* are preliminary and would require further exploration regarding the comparative behavior of the carrier and the loaded molecule as major aim for another

study, they still constitute the first report of a hybrid chromium-doped zinc gallate/mesoporous silica structure designed for both highly sensitive optical detection *in vivo* and drug delivery.

Conclusion. We introduced a novel generation of multifunctional nanoparticles that possess the ability to serve as both drug-delivery vehicle and optical imaging probe for *in vivo* applications. Based on a hybrid zinc gallate core/mesoporous silica shell architecture, these mesoporous persistent nanophosphors were shown to act as efficient drug loading/release vector for cytotoxic assay against U87MG cells. In addition to such therapeutic purpose, the inorganic core of this hybrid structure produces bright NIR persistent luminescence which allows highly sensitive detection through biological tissues. We demonstrated that the biodistribution of these drug-loaded mesoporous persistent nanophosphors could be easily monitored *in vivo* and return valuable information concerning the localization of the major drug-release area. This multifunctional breakthrough not only highlights the versatility of such persistent luminescence nanotechnology, but also gives access to a large field of promising biomedical applications in relation to both diagnostics and therapeutics.

ACKNOWLEDGMENT. We thank Corinne Chanéac, Domitille Giaume, and Xavier Pétrissans for their help and advices to perform N_2 adsorption/desorption isotherm measurements and analysis. We also thank R. Lai Kuen, B. Saubaméa, and J. Seguin for their contribution and help to perform transmission electron micrographs, *in vivo* experiments, and image analysis with Image J software. This work has been supported by the French National Agency (ANR) in the frame of its program in Nanosciences and Nanotechnologies (NATLURIM project n°ANR-08-NANO-025).

SUPPORTING INFORMATION AVAILABLE. BET plot curve of ZGO@SiO_2 nanoparticles, zeta potential data, absorption spectrum and releasing profile of doxorubicin in ZGO@SiO_2-Dox nanoparticles as well as biodistribution pattern 24h after intravenous injection in living mice are presented in supporting information. This material is available free of charge via the internet at http://pubs.acs.org

FIGURES.

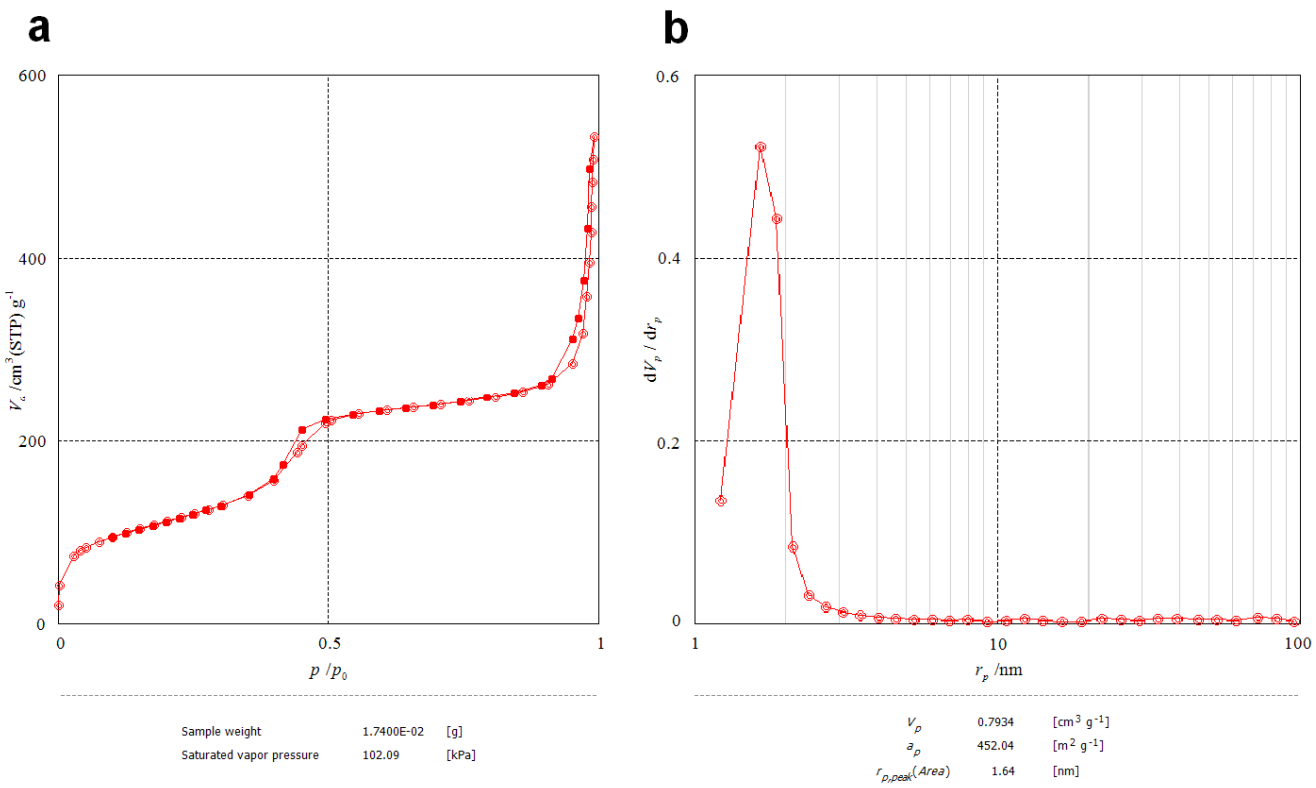

Figure 1. Porosity parameters of ZGO@SiO_2 nanoparticles following 6 extraction steps. **a**, N_2 adsorption-desorption isotherms. **b**, Size pore distribution in ZGO@SiO_2 nanoparticles calculated with the BJH method.

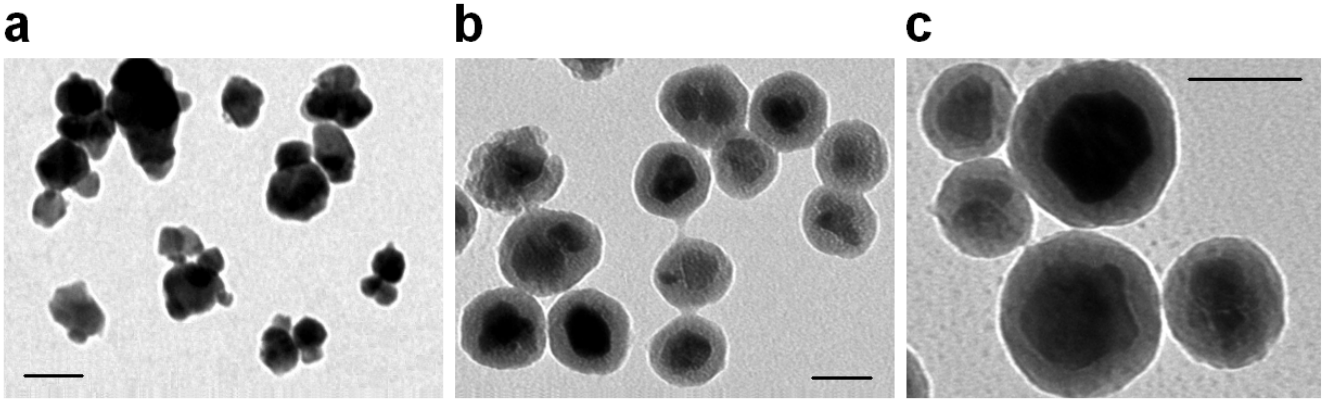

Figure 2. Transmission electron micrographs (TEM) of ZGO and ZGO@SiO_2 nanoparticles. **a**, TEM of ZGO nanoparticles (x 20000). **b**, TEM of ZGO@SiO_2 nanoparticles (x 20000). **c**, TEM of ZGO@SiO_2 nanoparticles (x 30000). Scale bars represent 50 nm.

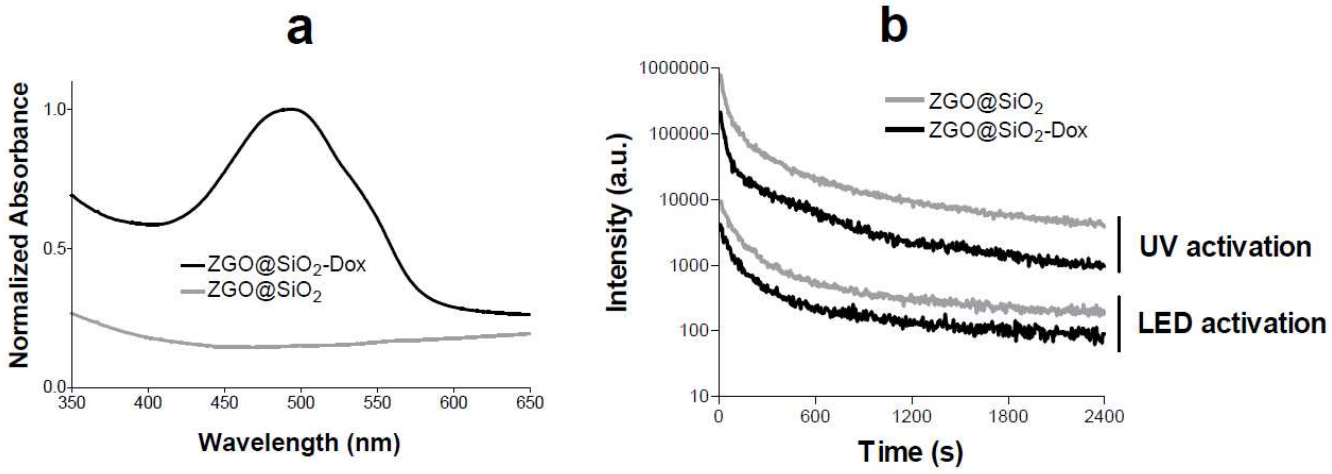

Figure 3. Optical properties of ZGO@SiO_2 and ZGO@SiO_2-Dox. **a**, Influence of doxorubicin loading on the absorbance of ZGO@SiO_2 nanoparticles. **b**, Persistent luminescence decay curves of ZGO@SiO_2 and ZGO@SiO_2-Dox nanoparticles after UV or LEDs excitation.

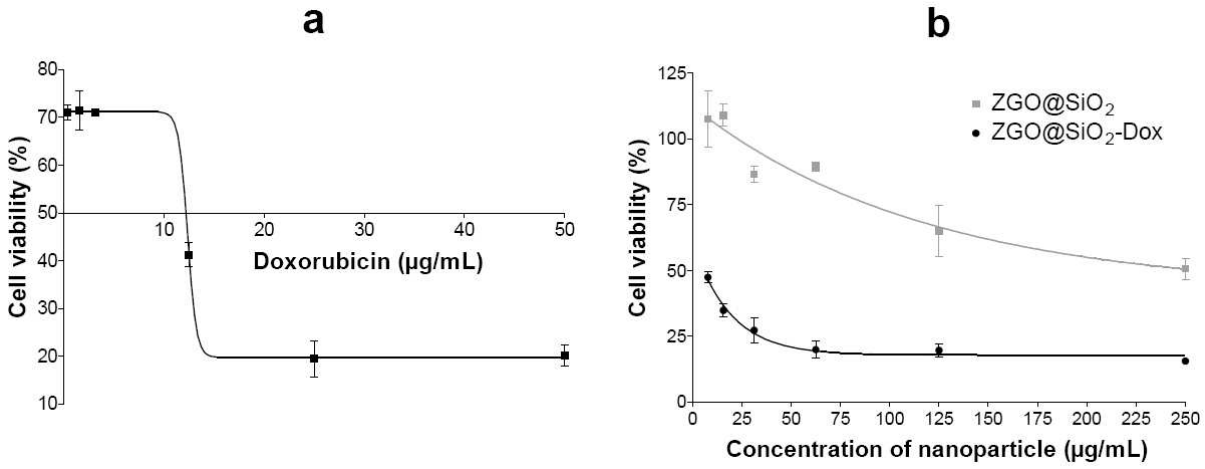

Figure 4. Relative cell viability of U87MG cells. **a**, After a 24 hours incubation period with free doxorubicin. **b**, After a 24 hours incubation period with either ZGO@SiO_2 or ZGO@SiO_2-Dox.

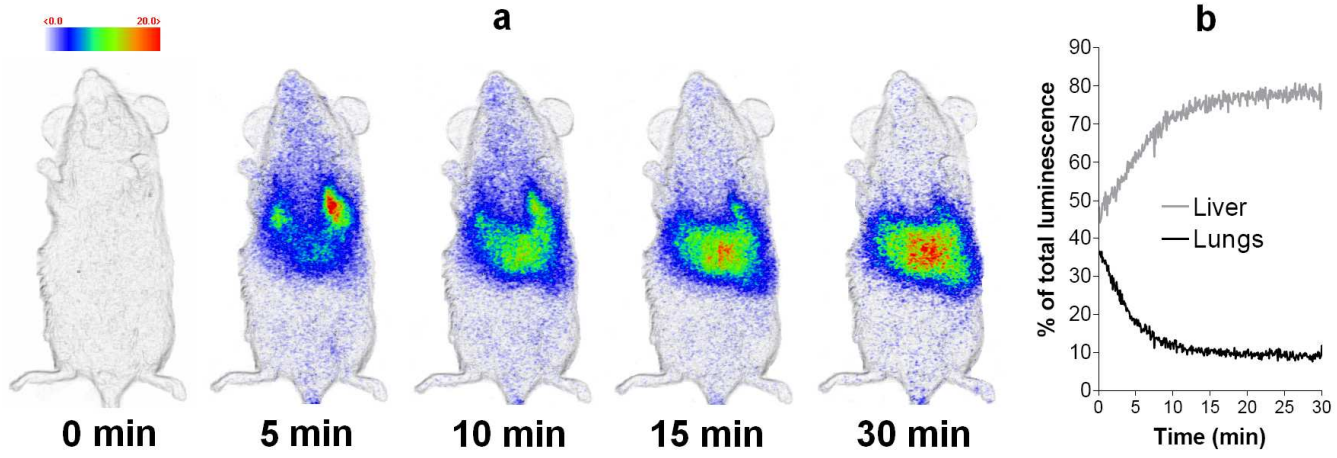

Figure 5. In vivo biodistribution of ZGO@SiO_2-Dox nanoparticles in mouse after intravenous injection. **a**, Persistent luminescence images up to 30 minutes after systemic injection (the blank mouse, before the injection, is referred to as "0 min"). **b**, Image-based semi-quantitation and time-dependent biodistribution within liver and lungs.

SCHEMES.

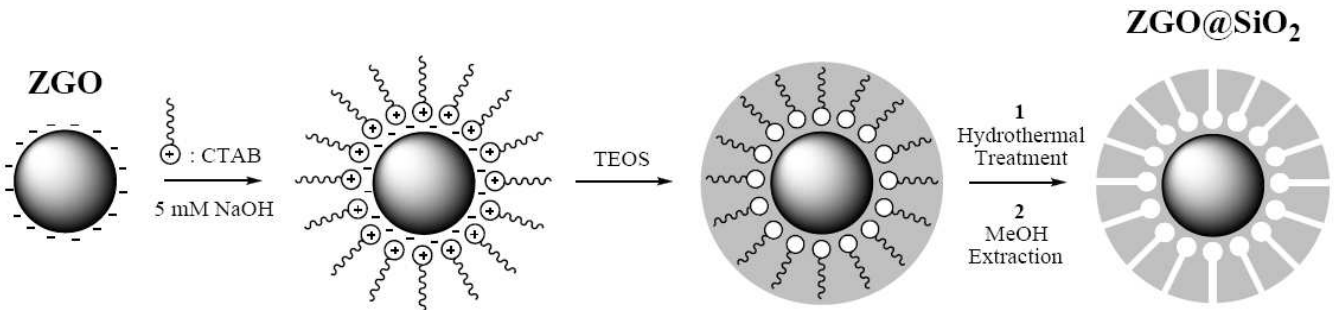

Scheme 1. Schematic representation of ZGO@SiO2 synthesis.

TABLES.

	BET specific surface area (m^2/g)	BJH specific surface area (m^2/g)	Average pore size (nm)
ZGO	28	28	6.95
ZGO@SiO_2 + 3 MeOH/NaCl extractions	171	159	1.64
ZGO@SiO_2 + 6 MeOH/NaCl extractions	411	452	1.64

Table 1. Porosity parameters following different steps of ZGO@SiO_2 synthesis.

	Hydrodynamic diameter (nm)	Zeta potential (mV)
ZGO	83,98 ± 0,61	22,2 ± 1,32
ZGO@SiO_2	162,7 ± 1,38	-27,1 ± 3,66
ZGO@SiO_2-DOX	184,9 ± 0,35	13,1 ± 0,56

Table 2. Physico-chemical characteristics of mesoporous persistent luminescence nanoparticles.

TOC GRAPHIC.

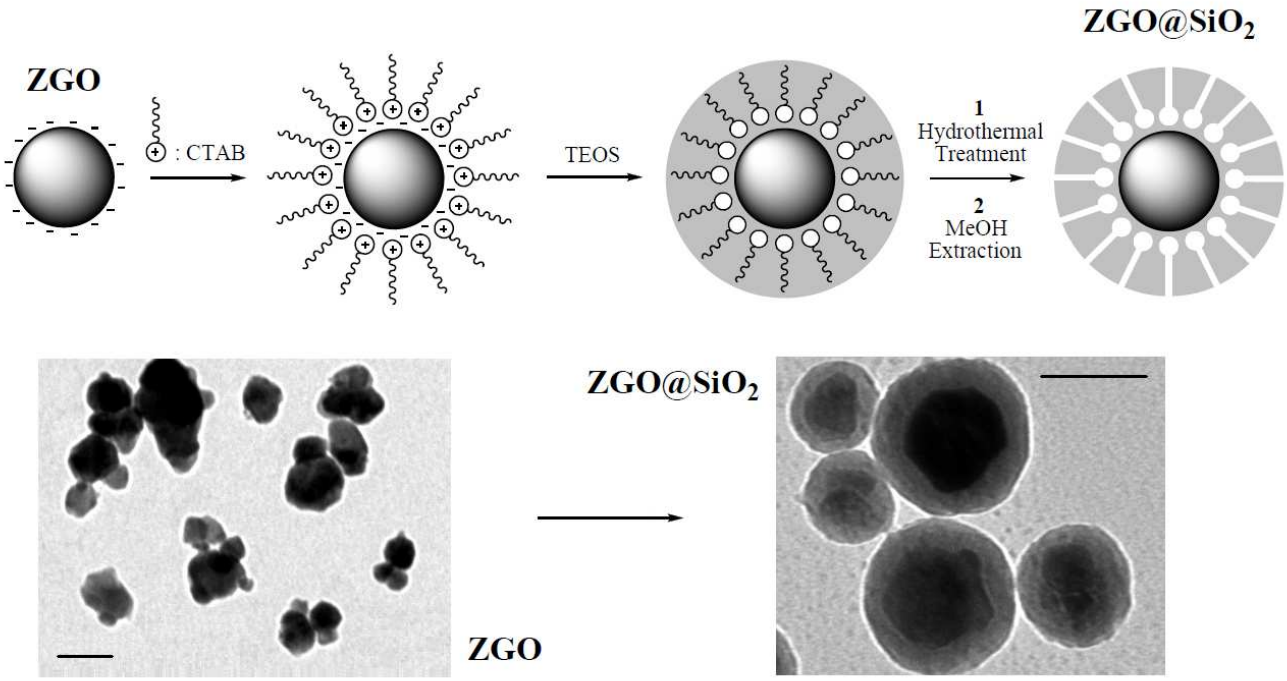

REFERENCES.

[1] Peer, D.; Karp, J.M.; Hong, S.; Farokhzad, O.C.; Margalit, R.; Langer, R. Nanocarriers as an emerging platform for cancer therapy. *Nat. Nanotechnol.* **2007,** 2(12), 751-60.

[2] Petros, R.A.; DeSimone, J.M. Strategies in the design of nanoparticles for therapeutic applications. *Nat. Rev. Drug Discov.* **2010,** 9(8), 615-27.

[3] Kelkar, S.S.; Reineke, T.M. Theranostics: combining imaging and therapy. *Bioconjug. Chem.* **2011,** 22(10), 1879-903.

[4] Chen, W.; Zhang, J. Using nanoparticles to enable simultaneous radiation and photodynamic therapies for cancer treatment. *J. Nanosci. Nanotechnol.* **2006,** 6(4), 1159-66.

[5] Choi, H.S.; Liu, W.; Misra, P.; Tanaka, E.; Zimmer, J.P.; Itty Ipe, B.; Bawendi, M.G.; Frangioni, J.V. Renal clearance of quantum dots. *Nat. Biotechnol.* **2007,** 25(10), 1165-70.

[6] Jokerst, J.V.; Lobovkina, T.; Zare, R.N.; Gambhir, S.S. Nanoparticle PEGylation for imaging and therapy. *Nanomedicine.* **2011,** 6(4), 715-28.

[7] Jain, R.K.; Stylianopoulos, T. Delivering nanomedicine to solid tumors. *Nat. Rev. Clin. Oncol.* **2010,** 7(11), 653-64.

[8] Xie, J.; Lee, S.; Chen, X. Nanoparticle-based theranostic agents. *Adv. Drug. Deliv. Rev.* **2010,** 62(11), 1064-79.

[9] Kim, J.; Kim, H.S.; Lee, N.; Kim, T.; Kim, H.; Yu, T.; Song, I.C.; Moon, W.K.; Hyeon, T. Multifunctional uniform nanoparticles composed of a magnetite nanocrystal core and a mesoporous silica shell for magnetic resonance and fluorescence imaging and for drug delivery. *Angew. Chem. Int. Ed. Engl.* **2008,** 47(44), 8438-41.

[10] Yang, P.; Gai, S.; Lin, J. Functionalized mesoporous silica materials for controlled drug delivery. *Chem. Soc. Rev.* **2012,** 41(9), 3679-98.

[11] Lee, J.E.; Lee, N.; Kim, T.; Kim, J.; Hyeon, T. Multifunctional mesoporous silica nanocomposite nanoparticles for theranostic applications. *Acc. Chem. Res.* **2011,** 44(10), 893-902.

[12] Gai, S. L.; Yang, P. P.; Li, C. X.; Wang, W. X.; Dai, Y. L.; Niu, N.; Lin, J. Synthesis of Magnetic, Up-Conversion Luminescent, and Mesoporous Core-Shell-Structured Nanocomposites as Drug Carriers. *Adv. Funct. Mater.* **2010**, 20, 1166-1172.

[13] Kim, T.; Momin, E.; Choi, J.; Yuan, K.; Zaidi, H.; Kim, J.; Park, M.; Lee, N.; McMahon, M.T.; Quinones-Hinojosa, A.; Bulte, J.W.; Hyeon, T.; Gilad, A.A. Mesoporous silica-coated hollow manganese oxide nanoparticles as positive T1 contrast agents for labeling and MRI tracking of adipose-derived mesenchymal stem cells. *J. Am. Chem. Soc.* **2011,** 133(9), 2955-61.

[14] Kim, J.; Lee, J.E.; Lee, J.; Yu, J.H.; Kim, B.C.; An, K.; Hwang, Y.; Shin, C.H.; Park, J.G.; Kim, J.; Hyeon, T. Magnetic fluorescent delivery vehicle using uniform mesoporous silica spheres embedded with monodisperse magnetic and semiconductor nanocrystals. *J. Am. Chem. Soc.* **2006,** 128(3), 688-9.

[15] Xu, Z.; Gao, Y.; Huang, S.; Ma, P.; Lin, J.; Fang, J. A luminescent and mesoporous core-shell structured Gd_2O_3:Eu^{3+}@nSiO_2@mSiO_2 nanocomposite as a drug carrier. *Dalton Trans.* **2011,** 40(18), 4846-54.

[16] Hu, X.; Zrazhevskiy, P.; Gao, X. Encapsulation of single quantum dots with mesoporous silica. *Ann. Biomed. Eng.* **2009,** 37(10), 1960-6.

[17] Kryza, D.; Taleb, J.; Janier, M.; Marmuse, L.; Miladi, I.; Bonazza, P.; Louis, C.; Perriat, P.; Roux, S.; Tillement, O.; Billotey, C. Biodistribution study of nanometric hybrid gadolinium oxide particles as a multimodal SPECT/MR/optical imaging and theragnostic agent. *Bioconjug. Chem.* **2011,** 22(6), 1145-52.

[18] Xu, Z.; Li, C.; Ma, P.; Hou, Z.; Yang, D.; Kang, X.; Lin, J. Facile synthesis of an up-conversion luminescent and mesoporous Gd_2O_3:Er^{3+}@nSiO_2@mSiO_2 nanocomposite as a drug carrier. *Nanoscale.* **2011,** 3(2), 661-7.

[19] le Masne de Chermont, Q.; Chanéac, C.; Seguin, J.; Pellé, F.; Maîtrejean, S.; Jolivet, J.P.; Gourier, D.; Bessodes, M.; Scherman, D. Nanoprobes with near-infrared persistent luminescence for in vivo imaging. *Proc. Natl. Acad. Sci. U S A.* **2007,** 104(22), 9266-71.

[20] Maldiney, T.; Sraiki, G.; Viana, B.; Gourier, D.; Richard, C.; Scherman, D.; Bessodes, M.; Van den Eeckhout, K.; Poelman, D.; Smet, P.F. In vivo optical imaging with rare earth doped $Ca_2Si_5N_8$ persistent luminescence nanoparticles. *Opt. Mater. Express.* **2012,** 2(3), 261-8.

[21] Maldiney, T.; Richard, C.; Seguin, J.; Wattier, N.; Bessodes, M.; Scherman, D. Effect of core diameter, surface coating, and PEG chain length on the biodistribution of persistent luminescence nanoparticles in mice. *ACS Nano.* **2011,** 5(2), 854-62.

[22] Jun, L.Z.; Wu, Z.H.; Meng, S.; Shan, S.J. and Xia, F.H. A facile and effective method to prepare long-persistent phosphorescent nanospheres and its potential application for in vivo imaging *J. Mater. Chem.* **2012,** 22, 24713.

[23] Maldiney, T.; Byk, G.; Wattier, N.; Seguin, J.; Khandadash, R.; Bessodes, M.; Richard, C.; Scherman, D. Synthesis and functionalization of persistent luminescence nanoparticles with small molecules and evaluation of their targeting ability. *Int. J. Pharm.* **2012,** 423(1), 102-7.

[24] Maldiney, T.; Kaikkonen, M.U.; Seguin, J.; le Masne de Chermont, Q.; Bessodes, M.; Airenne, K.J.; Ylä-Herttuala, S.; Scherman, D.; Richard, C. In vitro targeting of avidin-expressing glioma cells with biotinylated persistent luminescence nanoparticles. *Bioconjug. Chem.* **2012,** 23(3), 472-8.

[25] Wu, B.Y.; Wang, H.F.; Chen, J.T. & Yan, X.P. Fluorescence Resonance Energy Transfer Inhibition Assay for α-Fetoprotein Excreted during Cancer Cell Growth Using Functionalized Persistent Luminescence Nanoparticles. *J. Am. Chem. Soc.* **2011,** 133, 686-688.

[26] Maldiney, T.; Lecointre, A.; Viana, B.; Bessière, A.; Bessodes, M.; Gourier, D.; Richard, C.; Scherman, D. Controlling electron trap depth to enhance optical properties of persistent luminescence nanoparticles for in vivo imaging. *J. Am. Chem. Soc.* **2011,** 133(30), 11810-5.

[27] Liu, F.; Yan, W.; Chuang, Y.J.; Zhen, Z.; Xie, J.; Pan, Z. Photostimulated Near-Infrared Persistent Luminescence as a New Optical Read-Out from Cr^{3+}-Doped $LiGa_5O_8$. *Sci. Rep.* **2013,** 3, 1554-9.

[28] Abdukayum, A.; Chen, J.T.; Zhao, Q. and Yan, X.P. Functional near infrared-emitting Cr^{3+}/Pr^{3+} co-doped zinc gallogermanate persistent luminescent nanoparticles with superlong afterglow for in vivo targeted bioimaging, *J. Am. Chem. Soc.* **2013,** 135(38), 14125–14133.

[29] Maldiney, T.; Bessière, A.; Seguin, J.; Teston, E.; Sharma, S.K.; Viana, B.; Bos, A.J.; Dorenbos, P.; Bessodes, M.; Gourier, D.; Scherman, D.; Richard, C. The in vivo activation of persistent nanophosphors for optical imaging of vascularization, tumours and grafted cells. *Nat. Mater.* **2014,** 13(4), 418-426.

[30] Wu, S.H.; Hung, Y.; Mou, C.Y. Mesoporous silica nanoparticles as nanocarriers. *Chem. Commun (Camb).* **2011,** 47(36), 9972-85.

[31] Li, X.; Zhang, J.; Gu, H. Adsorption and desorption behaviors of DNA with magnetic mesoporous silica nanoparticles. *Langmuir.* **2011,** 27(10), 6099-106.

[32] Joo, S.H.; Park, J.Y.; Tsung, C.K.; Yamada, Y.; Yang, P.; Somorjai, G.A. Thermally stable Pt/mesoporous silica core-shell nanocatalysts for high-temperature reactions. *Nat. Mater.* **2009,** 8(2), 126-31.

[33] Kosmulski, M. Pristine Points of Zero Charge of Gallium and Indium Oxides. *J. Colloid Interface Sci.* **2001,** 238(1), 225-227.

[34] Kosmulski, M. The pH-dependent surface charging and points of zero charge: V. Update. *J. Colloid Interface Sci.* **2011,** 353(1), 1-15.

[35] Yuan, L.; Tang, Q.; Yang, D.; Zhang, J.Z.; Zhang, F.; Hu, J. Preparation of pH-Responsive Mesoporous Silica Nanoparticles and Their Application in Controlled Drug Delivery. *J. Phys. Chem. C.* **2011**, 115 (20), 9926-9932.

[36] Nair, K.L.; Jagadeeshan, S.; Nair, S.A.; Kumar, G.S. Evaluation of triblock copolymeric micelles of δ- valerolactone and poly (ethylene glycol) as a competent vector for doxorubicin delivery against cancer. *J. Nanobiotechnology.* **2011,** 9(42), 1-14.